FISEVIER

Contents lists available at ScienceDirect

Inorganica Chimica Acta

journal homepage: www.elsevier.com/locate/ica



Research paper

Heterobimetallic {PtMn} and {PtFe} lantern complexes with exceptionally long metallophilic contacts



Stephanie A. Beach^a, Linda A. Zuckerman^a, Romeo I. Portillo^b, Matthew P. Shores^b, Arnold L. Rheingold^c, Linda H. Doerrer^a

- ^a Department of Chemistry, Boston University, Boston, MA 02215, United States
- ^b Department of Chemistry, Colorado State University, Fort Collins, CO 80523-1872, United States
- ^c Department of Chemistry and Biochemistry, University of California, San Diego, 9500 Gilman Drive, MC 0332, La Jolla, CA 92093, United States

ABSTRACT

A new series of heterobimetallic lantern complexes, $[PtM(SAc)_4(pySMe)]$ (M = Mn (1), Fe (2), Co (3), Ni (4), Zn (5)), as well as additions to the previously reported series, $[PtM(SAc)_4(pyNH_2)]$ (M = Mn (6), Fe (7)), have been synthesized and thoroughly characterized. Notably, compounds 1 and 6 are the first crystallographically characterized, neutral Pt-Mn containing lantern complexes. Compounds 2 and 7 are the first examples of Pt-Fe containing lantern complexes with a pyridine based axial ligand. These newly synthesized complexes have been characterized by single-crystal X-ray diffraction and UV-vis (1–7), 1 H and 13 C NMR spectroscopies (5), and solution magnetic susceptibility (1–4 and 6–7) and analyzed in comparison to our previously reported lantern families. Compounds 2–4 are isomorphous and contain two crystallographically independent dimers with the same staggered conformations. One dimer has a typical Pt-···Pt metallophilic interaction ranging from 3.2198(6) to 3.2913(6) Å while the other has a much longer contact ranging from 3.3212(6) to 3.4533(6) Å. These latter contacts suggest metallophilic interactions that are the longest reported to date in any system. Solid state variable-temperature magnetic susceptibility studies suggest antiferromagnetic coupling between the 3*d* metal centers in the two lantern complexes of the dimeric forms of 2, 3, and 4.

1. Introduction

Synthetic chemists strive toward control over the magnetic and electronic properties of molecules. Many approaches have been employed in this pursuit, including modulation of metal-metal bonding and non-covalent interactions, as well as the installation of electronically conductive bridging ligands to link discrete units into quasi 1D arrays [1-5]. 1D systems are of interest due to their unique electronic [6] and magnetic properties [7] and notable potential applications in a variety of fields, including magnetic resonance (MR) imaging [8], vapochromic sensors [9], and luminescent materials [10,11]. Selectively controlling the magnetic and electronic properties of complexes through variations in the individual units is an active area of study. Heterobimetallic lantern (or paddlewheel) complexes of the form $[MM'(LX)_4(Y)_n]$, with M, M' = divalent metal, (LX) = chelating ligand, and Y a terminal ligand on M' as shown in the Scheme 1 inset, are attractive as their anisotropic structure enables such selectivity. The inherent donor atom asymmetry (L vs X) in these compounds can lead to tunable asymmetric electronic [12–14] and magnetic properties [15] depending on the choice of metal centers (M and M'), backbone ligand (L and X variations), and the terminal or bridging character of the axial

There are very few examples of heterobimetallic Fe- and Mn-

containing lantern complexes in the literature [16,17]. There are, however, many examples of homobimetallic monomeric and bridged lantern complexes supported through various neutral and anionic ligands as well as metal-metal interactions. Less common are Fe- and Mn-based lantern complexes. A handful of examples of homobimetallic Fe based lantern complexes were found through a search of the Cambridge Structural Database (CSD) [18]. For example, Lippard and colleagues have reported the synthesis of carboxylate rich {FeO₄} ligated di-iron monomers and dimeric species [19]. Within this work, it was demonstrated that the coordination of water alters the stereochemistry of a di-iron complex through the conversion of a lantern to a windmill geometry with two of the carboxylate ligands no longer bridging the iron centers, but instead each chelating to only one of the metal centers [20]. In addition to bimetallic lantern systems, Berry and colleagues have reported the synthesis and properties of Fe-containing trimeric lantern complexes that contain a quadruple bond, $M \equiv M \cdots M'$ (M = Cr, Mo, W; M' = Fe, Zn [21].

Similarly, a handful of homobimetallic and trimetallic Mn lantern complexes have been synthesized and characterized. Berry and coworkers reported a trimetallic $M_2M'(dpa)_4Cl_2$ (M = Cr, Mo; M' = Fe, Mn, dpa = 2,2'-dipyridylamide) lantern that demonstrates the effect of lattice solvent molecules and the large magnetic anisotropy of the quadruply bonded M centers on the relative zero field splitting of Fe vs Mn

E-mail address: doerrer@bu.edu (L.H. Doerrer).

4 HSAc + NaHCO₃ H₂O Pt M OH₂ pyNH₂ pyNH₂ reflux
$$M = Mn$$
 (6), Fe (7) acetone pySMe $M = Mn$ (1), Fe(2), Co (3), Ni (4), Zn (5)

Scheme 1. Heterobimetallic complexes synthesized with different axial ligands.

[22]. Carboxylate bridged bimetallic Mn-containing lanterns are also abundant, in both monomeric [23,24] and chain formations [25–27].

Based on a search of the CSD [18], there had been only one crystallographically-characterized heterobimetallic lantern structure that contains a Mn(II) center. This carboxylate based Pd-Mn lantern complex forms 1D arrays bridged through H-bonding of the axially coordinated water molecules and the MeCOOH lattice solvent molecules [16]. When searching for an Fe-containing heterobimetallic lantern, the only example found is a diamagnetic triply-bonded titanium/iron complex with no axially ligated terminal or bridging groups [17].

The only other examples of heterobimetallic lantern complexes containing Fe or Mn are from our own work. Previously, we have synthesized an anionic Mn-containing lantern, $\{Na(12C4)_2\}[PtMn(SAc)_4(NCS)], (12C4 = 12\text{-crown-4})$ [15]. This was the first example of a Mn lantern with an axially coordinated ligand, however only connectivity data could be collected from crystals of the complex and therefore it could not be fully compared to our previous complexes. The only other heterobimetallic Fe-containing lantern, $[PtFe(tba)_4(OH_2)]$ [28], had been previously synthesized and characterized, using the thiobenzoate (tba) backbone ligand as opposed to the thioacetate (SAc) used in the complexes described within this report.

Herein, we describe the synthesis and characterization of a new series of heterobimetallic lantern complexes $[PtM(SAc)_4(pySMe)]$ (pySMe = 4-thiomethylpyridine) in which M = Mn (1), Fe (2), Co (3), Ni (4), and Zn (5), as well as two new lantern complexes of the previously published $[PtM(SAc)_4(pyNH_2)]$ series [29] (SAc = thioacetate, pyNH₂ = 4-aminopyridine) in which M = Mn (6) and Fe (7). Compounds 1 and 6 are the first neutral Pt-Mn heterobimetallic lantern complexes to be prepared, the only other Pt-Mn example being our previously published anionic $\{Na(12C4)_2\}[PtMn(SAc)_4(NCS)]$ [15]. Additionally, 2 and 7 are the first examples of a Pt- and Fe-containing lantern structure with a substituted pyridine axial ligand.

2. General information

2.1. Materials and methods

Potassium tetrachloroplatinate (K₂PtCl₄) was prepared by a series of

literature procedures: platinum metal was dissolved in aqua regia to yield hexachloroplatinic acid ($\rm H_2PtCl_6$) [30], which was converted to potassium hexachloroplatinate ($\rm K_2PtCl_6$) by a cation exchange [31], followed by reduction of $\rm K_2PtCl_6$ to $\rm K_2PtCl_4$ [32]. Other reagents were obtained commercially and used without further purification. The ligand 4-(methylsulfanyl)pyridine (CAS: 22581-72-2), was purchased from Enamine at 95% purity and used without further purification. Elemental analyses were performed by Atlantic Microlab Inc. (Norcross, GA). UV–vis–NIR spectra were measured with a Shimadzu UV-3600 spectrometer. 1 H- and 13 C(1 H)-NMR spectra measurements were recorded on a Varian 500 MHz spectrometer. NMR spectra for 5 are presented in Fig. S1 (1 H) and Fig. S2 (13 C).

2.2. X-ray crystallography

Crystals of 1–7 were mounted on a Cryoloop with Paratone N oil, and data were collected at 100 K on a Bruker Proteum-R with a CCD detector using Mo K α radiation (1–5, 7) or Cu K α radiation (6). A summary of crystal data collection and refinement parameters for all compounds is found in Table S1. Selected bond distances and angles for 1 and 5–7 are found in Table S2 while non-hydrogen distances and angles for all complexes can be found in Tables S3–9. Data were corrected for absorption with SADABS and structures were solved by direct methods. All non-hydrogen atoms were refined anisotropically by full matrix least-squares on F^2 .

2.3. Magnetism

Solution-state magnetic susceptibilities were collected with the Evans method [33,34]. Solid-state magnetic property data for compounds 2–4 were collected using a Quantum Design MPMS XL magnetometer. Powdered microcrystalline samples were loaded into polyethylene bags and inserted into straws before transportation to the magnetometer. The presence of ferromagnetic impurities was probed by a variable field analysis (0–10 kOe) of the magnetization at 100 K (Figs. S12–S14). Lack of curvature in the *M* vs *H* plots for 3 and 4 (Figs. S13 and S14) indicate the absence of significant ferromagnetic impurities; the curve in low field portion of the *M* vs *H* plot for 2 (Fig. S12)

obligates the use of higher fields ($H \ge 1$ kOe) for further measurements. Magnetic susceptibility data were collected at temperatures ranging from 2 to 300 K. Data were corrected for the diamagnetic contributions of the sample holder and bag by subtracting empty containers; corrections for the sample were calculated from Pascal's constants [35]. The magnetic susceptibility data were fit to spin Hamiltonians of general form $\hat{H} = -2J(\hat{S}_i \cdot \hat{S}_i)$ using the program PHI [36].

3. Experimental

3.1. Synthesis of $[PtM(SAc)_4(pySMe)]$ (M = Mn, Fe, Co, Ni, Zn)

The starting complexes [PtM(SAc)₄(OH₂)], M = Mn [15], Fe, Co, Ni, Zn were prepared by previously reported methods [13]. Although commonly reported in units of Bohr magneton, μ_B , effective magnetic moments are unitless [37,38].

3.1.1. To obtain $[PtMn(SAc)_4(pySMe)]$ (1)

[PtMn(SAc)₄(OH₂)] (109.5 mg, 0.193 mmol) was freshly prepared with MnSO₄·H₂O as the 3*d* metal source and dissolved in ~5 mL of acetone. An amount of pySMe (24 mg, 0.192 mmol) was dissolved in ~5 mL acetone and added dropwise to the above mixture. After stirring for 24 h at room temperature, an off-white precipitate was filtered from a colorless solution, and washed with hexanes. The solid was recrystallized from CH₂Cl₂ slow evaporation at ~9 °C to obtain analytically pure pale yellow crystals of the composition [PtMn (SAc)₄(pySMe)]. Recrystallized yield: 34.2%. Anal. Calc'd. for PtMnC₁₄H₁₉NO₄S₅: C, 24.89; H, 2.83; N, 2.07%. Found: C, 24.95; H, 2.81; N, 2.10%. UV-vis–NIR (CH₂Cl₂) (λ _{max}, nm (ϵ _M, cm⁻¹ M⁻¹)): 273(84,700), 357 sh(3220). Evans method (CD₂Cl₂): 5.8(1).

3.1.2. To obtain $[PtFe(SAc)_4(pySMe)]$ (2)

[PtFe(SAc)₄(OH₂)] was freshly prepared with FeSO₄·7H₂O as the 3*d* metal source and the above synthesis for [PtMn(SAc)₄(pySMe)], was executed. An orange solid was obtained and recrystallized from slow evaporation of CH₂Cl₂ at \sim 9 °C to obtain analytically pure orange crystals of the composition [PtFe(SAc)₄(pySCH₃)]. Recrystallized yield: 48.9%. Anal. Calc'd. for PtFeC₁₄H₁₉NO₄S₅: C, 24.86; H, 2.83; N, 2.07%. Found: C, 25.16; H, 2.82; N, 1.99%. UV–vis–NIR (CH₂Cl₂) (λ _{max}, nm (ϵ _M, cm⁻¹ M⁻¹)): 274(88,500), 380(3060), 970(8). Evans method (CD₂Cl₂): 5.5(1).

3.1.3. To obtain $[PtCo(SAc)_4(pySMe)]$ (3)

[PtCo(SAc)₄(OH₂)] was freshly prepared with CoCl₂·6H₂O as the 3*d* metal source and the above synthesis for [PtMn(SAc)₄(pySMe)], was executed. Pale purple crystals suitable for X-ray crystallography were grown from the slow evaporation of CH₂Cl₂ at ~9 °C in 54.7% recrystallized yield. Anal. Calc'd. for PtCoC₁₄H₁₉NO₄S₅: C, 24.74; H, 2.82; N, 2.06%. Found: C, 24.52; H, 2.80; N 1.98%. UV–vis–NIR (CH₂Cl₂) (λ_{max} , nm (ϵ_{M} , cm⁻¹ M⁻¹)): 279 (51100), 499(123), 524(70.3), 583(20.8), 1383(5). Evans method (CD₂Cl₂): 5.2(1).

3.1.4. To obtain $[PtNi(SAc)_4(pySMe)]$ (4)

[PtNi(SAc)₄(OH₂)] was freshly prepared with NiCl₂·6H₂O as the 3d metal source and the above synthesis for [PtMn(SAc)₄(pySMe)], was executed. A yellow-green solid was obtained and recrystallized from CH₂Cl₂ slow evaporation at ~9 °C to obtain analytically pure green crystals of the composition [PtNi(SAc)₄(pySMe)]. Recrystallized yield: 48.4%. Anal. Calc'd. for PtNiC₁₄H₁₉NO₄S₅: C, 24.75; H, 2.82; N, 2.06%. Found: C, 24.80; H, 2.74; N, 2.00%. UV-vis-NIR (CH₂Cl₂) (λ _{max}, nm (ϵ _M, cm⁻¹ M⁻¹)): 275(76,200), 673(10), 830(2), 1165(9). Evans method (CD₂Cl₂): 3.8(1).

3.1.5. To obtain $[PtZn(SAc)_4(pySMe)]$ (5)

[PtZn(SAc)₄(OH₂)] was freshly prepared with ZnCl₂ as the 3d metal

source and the above synthesis for [PtMn(SAc)₄(pySMe)] was executed. A white solid was obtained and recrystallized from CH₂Cl₂ slow evaporation at ~9 °C to obtain analytically pure white crystals of the composition [PtZn(SAc)₄(pySMe)]. Recrystallized yield: 51.7%. Anal. Calc'd. for PtZnC₁₄H₁₉NO₄S₅: C, 24.51; H, 2.79; N, 2.04%. Found: C, 24.70; H, 2.75; N, 2.14%. UV–vis–NIR (CH₂Cl₂) (λ_{max} , nm (ϵ_{M} , cm⁻¹ M⁻¹)): 276(56,600). ¹H NMR (δ , ppm {CD₂Cl₂}: 2.38 (s, 12H, CCH₃), 2.58 (s, 3H, SCH₃), 8.65 (d, 4H, NC₅H₄SMe). ¹³C NMR (δ , ppm {CD₂Cl₂}): 214.6 (s, SO(C)CH₃), 155.76 (s, para-NC₅H₄SMe), 147.98 (s, ortho-NC₅H₄SMe), 120.45 (s, meta-NC₅H₄SMe), 32.59 (s, SO(C)CH₃), 13.75 (s, SCH₃).

3.2. Synthesis of $[PtM(SAc)_4(pyNH_2) (M = Fe, Mn)]$

The starting materials $[PtM(SAc)_4(pyNH_2)]$ with M=Mn and Fe were prepared as described above.

3.2.1. To obtain [PtMn(SAc)₄(pyNH₂)] (6)

Freshly prepared [PtMn(SAc)₄(OH₂)] (110 mg, 0.193 mmol) was dissolved in $\sim\!20\,\text{mL}$ of acetone and added to 10 mL of CH₂Cl₂. An amount of pyNH₂ (18.1 mg, 0.192 mmol) was dissolved in $\sim\!10\,\text{mL}$ of CH₂Cl₂ and added to the above mixture. The reaction mixture was refluxed for 3 h and concentrated to $\sim\!5\,\text{mL}$ of solvent, which caused a substantial amount of off-white precipitate to form. The solid was removed by filtration, washed with Et₂O, and dried in vacuo. Pale yellow X-ray quality crystals were grown from CH₂Cl₂ layered with hexanes at $\sim\!9\,^\circ\text{C}$, resulting in 29.9% yield of the composition [PtMn (SAc)₄(pyNH₂)]. Anal. Calc'd. for PtMnC₁₃H₁₈N₂O₄S₄: C, 24.22; H, 2.81; N, 4.35%. Found: C, 24.50; H, 2.82; N, 4.55%. UV–vis–NIR (CH₂Cl₂) (λ_{max} , nm (ϵ_{M} , cm $^{-1}$ M $^{-1}$)): 271(68,200), 362(22,500). Evans method (CD₂Cl₂): 5.9(1).

3.2.2. To obtain $[PtFe(SAc)_4(pyNH_2)]$ (7)

[PtFe(SAc)₄(OH₂)] was freshly prepared with FeSO₄:7H₂O as the metal source and the above synthesis for [PtMn(SAc)₄(pyNH₂)] was executed. Orange X-ray quality crystals were grown from CH₂Cl₂ layered with hexanes, resulting in 30.6% yield of the composition [PtFe (SAc)₄(pyNH₂)]. Anal. Calc'd. for PtFeC₁₃H₁₈N₂O₄S₄: C, 24.19; H, 2.81; N, 4.34%. Found: C, 24.32; H, 2.78; N, 4.36%. UV–vis–NIR (CH₂Cl₂) (λ_{max} , nm (ϵ_{M} , cm⁻¹ M⁻¹)): 250(73,300), 359(15,900). Evans method (CD₂Cl₂): 4.4(1).

4. Results and discussion

4.1. Synthesis and structure

The utility of the thioacetate ligand for selective coordination of two different metals has been well shown in our previous work [39]. The lantern complexes reported herein were synthesized through modification of our previously published methods, as seen in Scheme 1, using metal salt hydrates of MnSO $_4$ due to its availability for 1 and 6, and FeSO $_4$ as opposed to the more easily oxidized chloride salt for 2 and 7

All of the presented complexes were synthesized from freshly prepared [PtM(SAc)_4(OH_2)] [13]. For the synthesis of 1–5, the water adduct is dissolved in approximately 5 mL of acetone to which pySMe dissolved in ~ 5 mL acetone is added dropwise. This solution is then stirred for 24 h at room temperature, yielding a precipitate that is isolated via filtration. The collected solid is then washed with hexanes and crystallized via slow evaporation of CH₂Cl₂. Compounds 6 and 7 were similarly synthesized by dissolving the freshly prepared water adduct in a mixture of 20 mL of acetone and 10 mL of CH₂Cl₂ and then adding pyNH₂ dissolved in 10 mL of CH₂Cl₂. The resultant mixture is refluxed for approximately three hours after which the solution is concentrated and the precipitate collected by filtration, and this powder is then rinsed with Et₂O, dried, and crystallized via CH₂Cl₂ slow evaporation.

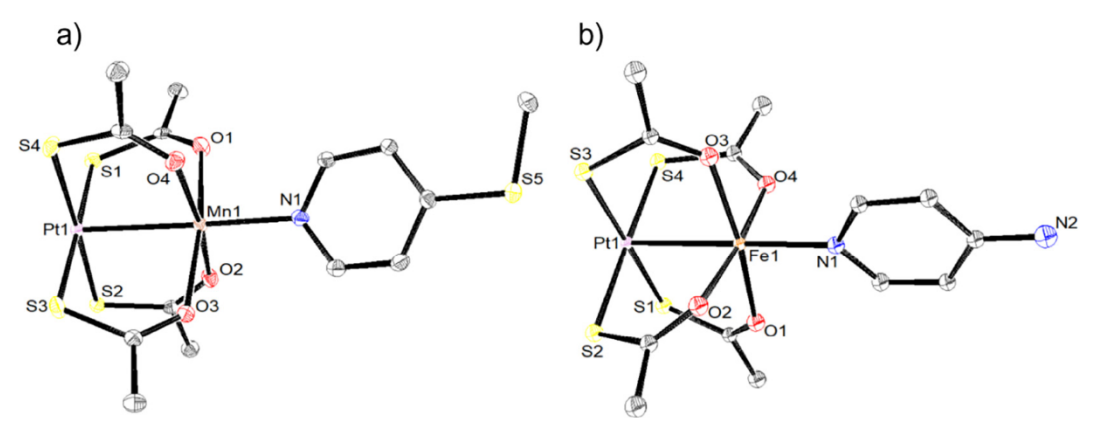


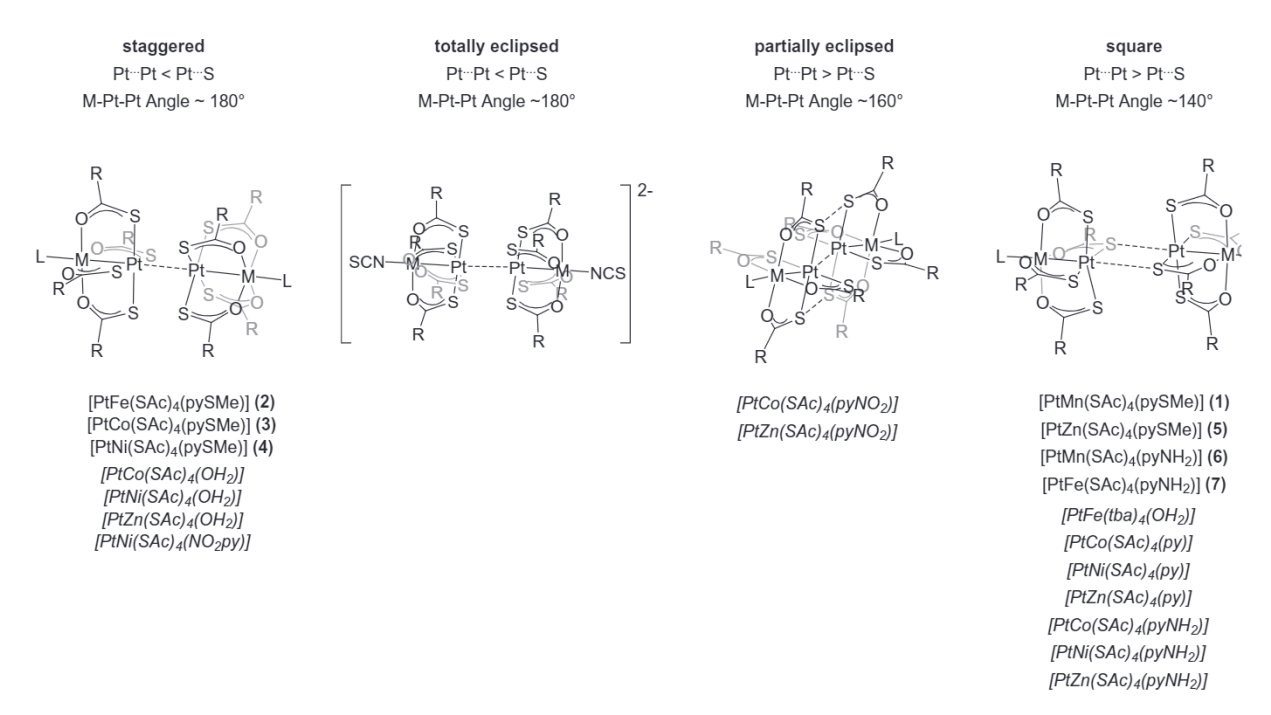
Fig. 1. ORTEP of [PtMn(SAc)₄(pySMe)] (1) and [PtFe(SAc)₄(pyNH₂)] (7). Ellipsoids are drawn at the 50% level. Hydrogen atoms and solvent molecules are omitted for clarity.

Compounds 1 and 6 are the first examples of a neutral Pt-Mn lantern with an axial ligand, and the first to be crystallographically well-characterized, as seen in Fig. 1. The first reported example of a Pt-Mn lantern was $\{Na(12C4)_2\}[PtMn(SAc)_4(NCS)]$, which was prepared by our group with thiocyanate (NCS^-) in the axial position, resulting in an anionic species charge-balanced by $[\{Na(12C4)_2\}]^+$ [15]. Single crystals of this complex were obtained but due to excessive solvent disorder only connectivity information could be determined from the single crystal X-ray diffraction data. Compound 1 was found to have a non-bonding Pt---Pt interaction of 3.8104(3) Å and Pt---S interaction of 3.2896(7) Å.

We have previously shown that in the solid state, the intermolecular Pt···Pt and Pt···S interactions of these lantern complexes can lead to dimeric species, which have been divided into four different categories based on these distances as well as the angle along the M-Pt-Pt vector [15,29]. These designations are shown in Scheme 2 with the metrical parameters used to distinguish them, including the new compounds reported herein, as well as compounds with terminal water [13], nitropyridine [13], pyridine [29], and 4-aminopyridine ligands from previous publications [29]. The solid-state dimer of 1 falls into the

previously determined square classification, as seen in Scheme 2. However, 1 has a M-Pt-Pt angle of approximately 150°, the largest of any lantern in the square class. All other square lantern complexes have angles close to 140° and show a linear decrease of this angle with the decreasing intermolecular S···S contact, as seen in Fig. 2. It has been previously observed that as the M-Pt-Pt angle becomes more acute, the sulfur atoms are brought into closer contact, but this is not the case for 1, perhaps due to differences in the crystal packing.

Compounds 2 and 7 are the first examples of a Pt-Fe lantern with a pyridine-based axial ligand. The only previously published Pt-Fe containing lantern complex, [PtFe(tba)_4(OH_2)] [28], was synthesized by our group with a thiobenzoate backbone ligand and its solid state dimer exhibited the square conformation. Single crystal X-ray diffraction studies of Fe-containing 2 revealed two crystallographically independent dimers with Pt-Fe distances of 2.6848(8) Å and 2.6633(8) Å, as shown in Fig. 3 and Table 1. The B/C dimer has longer Pt-Fe distances with an intermolecular Pt(1B)···Pt(1C) interaction of 3.2913(6) Å, suggesting a Pt···Pt metallophilic interaction, the first time a metallophilic interaction has been observed between any {PtFe} hetero-bimetallic lantern complexes.



Scheme 2. Solid state dimeric lantern classifications of dimeric $[PtM(LX)_4(L)]$ complexes with substituted pyridine or water axial ligands. Compounds in italics have been previously reported.

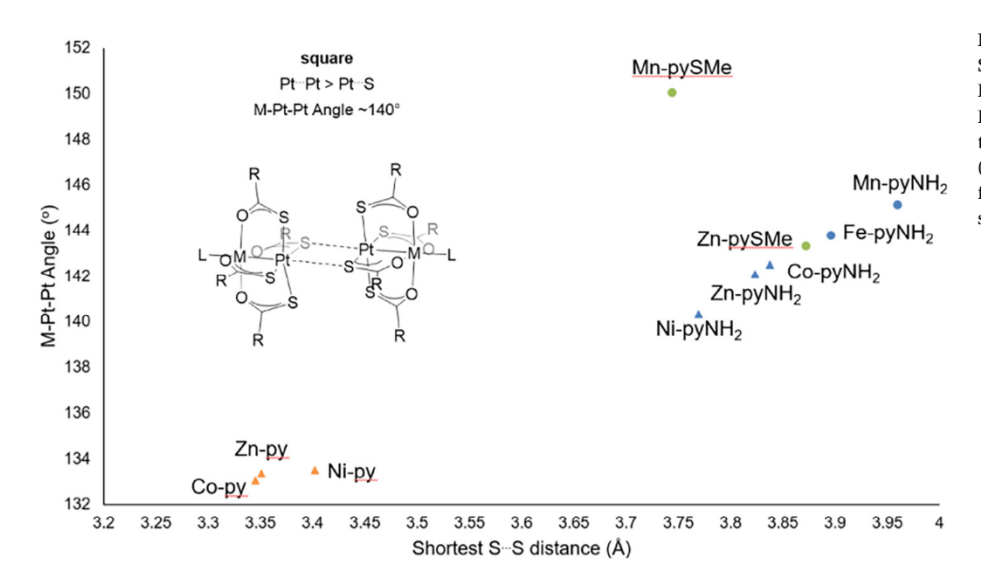


Fig. 2. Comparison of M-Pt-Pt angle and shortest $S\cdots S$ contact in square lantern complexes when L=py (orange), $pyNH_2$ (blue), pySMe (green). Previously published complexes are denoted with triangles while 1,5,6 and 7 are denoted with circles. (For interpretation of the references to colour in this figure legend, the reader is referred to the web version of this article.)

The Pt(1A)···Pt(1D) distance in the A/D dimer of **2** has a much longer Pt···Pt interaction of 3.4533(6) Å. Interestingly, both independent dimers seen in the crystal structure fall into the staggered category, with Pt···Pt interactions shorter than Pt···S and virtually linear Fe-Pt-Pt vectors, as opposed to the previously observed square classification for a Fe-containing lantern complex [28]. This longer dimer is significant, as previously all the staggered lantern complexes have distances consistent with Pt···Pt metallophilic interactions within the range of 3.0583(4)–3.1261(3) Å. Given the structural variability in

these dimers, Scheme 2, this linear arrangement of the four metal centers seems to indicate a direct interaction of the two Pt atoms even at a long distance, which is preferred for the staggered complexes over any other structure. The staggering of the carboxylate backbone ligands allows for the much closer Pt interactions observed in these complexes and promotes greater overlap of the d_z^2 orbitals. Despite these much longer than usual Pt···Pt interactions, the staggered conformation of both dimers leads to their metallophilic classification and displays the subtle energy differences between and within the four classes of lantern

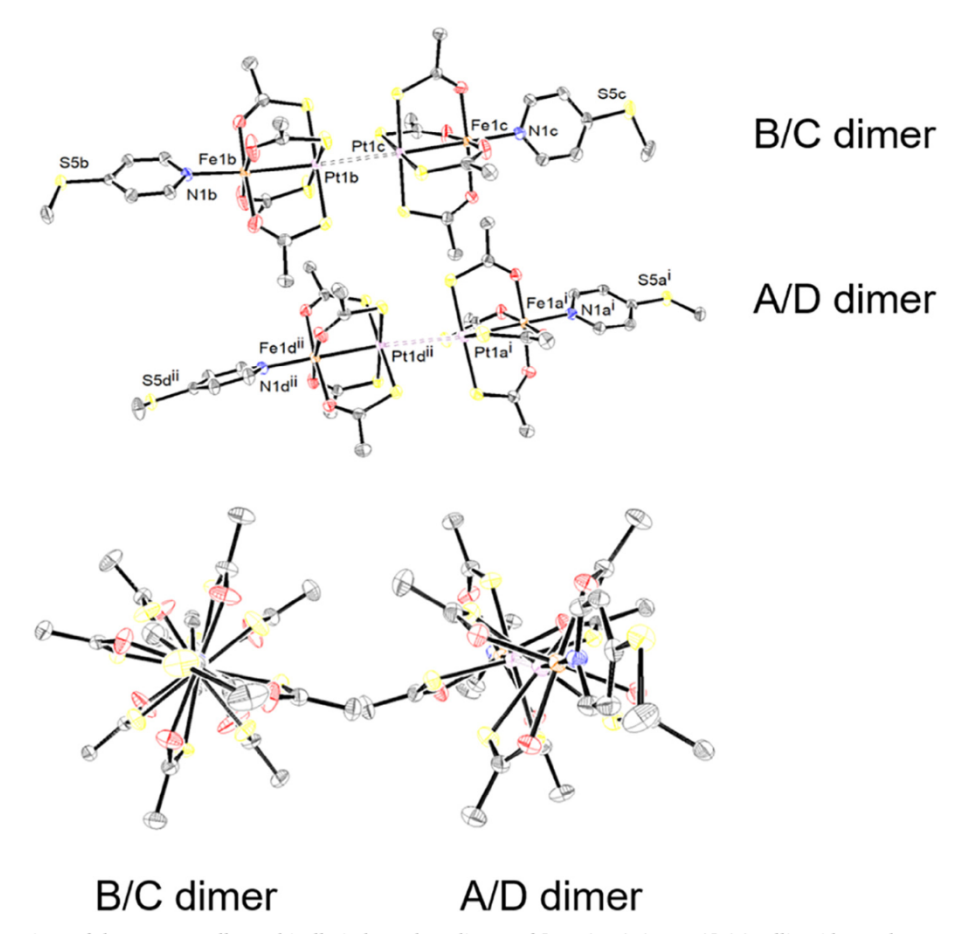


Fig. 3. Staggered conformations of the two crystallographically independent dimers of [PtFe(SAc)₄(pySMe)] (2). Ellipsoids are drawn at the 50% level. Hydrogen atoms and solvent molecules are omitted for clarity.

Table 1
Selected bond distances (Å) and interatomic angles (°) for 2–4.

2		3		4	
Pt-Fe (1A)	2.6633(6)	Pt-Co (1A)	2.6477(13)	Pt-Ni (1A)	2.5918(4)
Pt-Fe (1B)	2.6737(6)	Pt-Co (1B)	2.6431(13)	Pt-Ni (1B)	2.6057(4)
Pt-Fe (1C)	2.6848(6)	Pt-Co (1C)	2.6566(13)	Pt-Ni (1C)	2.6166(4)
Pt-Fe (1D)	2.6762(6)	Pt-Co (1D)	2.6339(13)	Pt-Ni (1D)	2.5945(4)
Pt-Fe (1A)	0.0018	Pt-Co (1A)	0.00091	Pt-Ni (1A)	0.0032
Pt-Fe (1B)	0.0042	Pt-Co (1B)	0.00013	Pt-Ni (1B)	0.0028
Pt-Fe (1C)	0.0048	Pt-Co (1C)	0.00078	Pt-Ni (1C)	0.0024
Pt-Fe (1D)	0.0012	Pt-Co (1D)	0.00117	Pt-Ni (1D)	0.002
Fe-N (1A)	2.121(3)	Co-N (1A)	2.084(8)	Ni-N (1A)	2.040(3)
Fe-N (1B)	2.131(3)	Co-N (1B)	2.089(8)	Ni-N (1B)	2.038(3)
Fe-N (1C)	2.132(3)	Co-N (1C)	2.100(8)	Ni-N (1C)	2.049(3)
Fe-N (1D)	2.127(3)	Co-N (1D)	2.089(8)	Ni-N (1D)	2.042(3)
Fe-N (1A)	0.003	Co-N (1A)	0.032	Ni-N (1A)	0.027
Fe-N (1B)	0.003	Co-N (1B)	0.072	Ni-N (1B)	0.024
Fe-N (1C)	0.006	Co-N (1C)	0.072	Ni-N (1C)	0.027
Fe-N (1D)	0.021	Co-N (1D)	0.072	Ni-N (1D)	0.006
Pt(1B)Pt(1C)	3.2913(6)	Pt(1B)Pt(1C)	3.2737(7)	Pt(1C)Pt(1D)	3.2198(6)
Pt(1A)···Pt(1D)	3.4533(6)	Pt(1A)Pt(1D)	3.3977(7)	Pt(1A)Pt(1B)	3.3212(6)
Fe(1C)-Pt(1C)-Pt(1B)	177.63(2)	Co(1C)-Pt(1C)-Pt(1B)	178.09(3)	Ni(1D)-Pt(1D)-Pt(1C)	178.06(2)
Fe(1D)-Pt(1D)-Pt(1A)	175.01(2)	Co(1A)-Pt(1)-Pt(1D)	175.64(3)	Ni(1B)-Pt(1B)-Pt(1A)	176.25(2)
B/C dimer	4.031	B/C dimer	4.019	C/D dimer	3.981
,		,		,	4.071
	Pt-Fe (1A) Pt-Fe (1B) Pt-Fe (1C) Pt-Fe (1D) Pt-Fe (1D) Pt-Fe (1B) Pt-Fe (1B) Pt-Fe (1C) Pt-Fe (1D) Fe-N (1A) Fe-N (1B) Fe-N (1C) Fe-N (1D) Fe-N (1B) Fe-N (1C) Fe-N (1D) Ft(1B)	Pt-Fe (1A) 2.6633(6) Pt-Fe (1B) 2.6737(6) Pt-Fe (1C) 2.6848(6) Pt-Fe (1D) 2.6762(6) Pt-Fe (1A) 0.0018 Pt-Fe (1B) 0.0042 Pt-Fe (1B) 0.0012 Fe-N (1A) 2.121(3) Fe-N (1B) 2.131(3) Fe-N (1B) 2.131(3) Fe-N (1C) 2.132(3) Fe-N (1D) 2.127(3) Fe-N (1D) 2.127(3) Fe-N (1B) 0.003 Fe-N (1B) 0.003 Fe-N (1B) 0.003 Fe-N (1C) 0.006 Fe-N (1D) 0.021 Pt(1B)Pt(1C) 3.2913(6) Pt(1A)Pt(1D) 3.4533(6) Fe(1C)-Pt(1C)-Pt(1B) 177.63(2) Fe(1D)-Pt(1D)-Pt(1A) 175.01(2) B/C dimer 4.031	Pt-Fe (1A) 2.6633(6) Pt-Co (1A) Pt-Fe (1B) 2.6737(6) Pt-Co (1B) Pt-Fe (1C) 2.6848(6) Pt-Co (1C) Pt-Fe (1D) 2.6762(6) Pt-Co (1D) Pt-Fe (1D) 0.0018 Pt-Co (1A) Pt-Fe (1B) 0.0042 Pt-Co (1B) Pt-Fe (1C) 0.0048 Pt-Co (1C) Pt-Fe (1D) 0.0012 Pt-Co (1D) Fe-N (1A) 2.121(3) Co-N (1A) Fe-N (1B) 2.131(3) Co-N (1B) Fe-N (1C) 2.132(3) Co-N (1C) Fe-N (1D) 2.127(3) Co-N (1D) Fe-N (1D) 2.127(3) Co-N (1D) Fe-N (1B) 0.003 Co-N (1A) Fe-N (1B) 0.003 Co-N (1B) Fe-N (1B) 0.003 Co-N (1B) Fe-N (1D) 0.021 Co-N (1D) Pt(1B)Pt(1C) 3.2913(6) Pt(1B)Pt(1C) Pt(1A)Pt(1D) 3.4533(6) Pt(1A)Pt(1D) Pt(1C)-Pt(1C)-Pt(1B) 177.63(2) Co(1C)-Pt(1C)-Pt(1B)	Pt-Fe (1A) 2.6633(6) Pt-Co (1A) 2.6477(13) Pt-Fe (1B) 2.6737(6) Pt-Co (1B) 2.6431(13) Pt-Fe (1C) 2.6848(6) Pt-Co (1C) 2.6566(13) Pt-Fe (1D) 2.6762(6) Pt-Co (1D) 2.6339(13) Pt-Fe (1A) 0.0018 Pt-Co (1A) 0.00091 Pt-Fe (1B) 0.0042 Pt-Co (1B) 0.00013 Pt-Fe (1C) 0.0048 Pt-Co (1C) 0.00078 Pt-Fe (1D) 0.0012 Pt-Co (1D) 0.00117 Fe-N (1A) 2.121(3) Co-N (1A) 2.084(8) Fe-N (1B) 2.131(3) Co-N (1B) 2.089(8) Fe-N (1C) 2.132(3) Co-N (1C) 2.100(8) Fe-N (1D) 2.127(3) Co-N (1D) 2.089(8) Fe-N (1A) 0.003 Co-N (1D) 2.089(8) Fe-N (1B) 0.003 Co-N (1B) 0.072 Fe-N (1B) 0.003 Co-N (1B) 0.072 Fe-N (1D) 0.021 Co-N (1D) 0.072 Fe-N (1D) 0	Pt-Fe (1A) 2.6633(6) Pt-Co (1A) 2.6477(13) Pt-Ni (1A) Pt-Fe (1B) 2.6737(6) Pt-Co (1B) 2.6431(13) Pt-Ni (1B) Pt-Fe (1C) 2.6848(6) Pt-Co (1C) 2.6566(13) Pt-Ni (1C) Pt-Fe (1D) 2.6762(6) Pt-Co (1D) 2.6339(13) Pt-Ni (1D) Pt-Fe (1D) 0.0018 Pt-Co (1A) 0.00091 Pt-Ni (1A) Pt-Fe (1B) 0.0042 Pt-Co (1B) 0.00013 Pt-Ni (1B) Pt-Fe (1D) 0.0012 Pt-Co (1C) 0.00078 Pt-Ni (1C) Pt-Fe (1D) 0.0012 Pt-Co (1D) 0.00117 Pt-Ni (1D) Pt-Fe (1D) 0.0012 Pt-Co (1D) 0.00117 Pt-Ni (1D) Pt-Fe (1D) 0.0012 Pt-Co (1D) 0.00117 Pt-Ni (1D) Pt-Fe (1D) 0.0012 Co-N (1A) 2.084(8) Ni-N (1A) Pt-N (1A) 2.131(3) Co-N (1B) 2.089(8) Ni-N (1C) Pt-N (1C) 2.132(3) Co-N (1C) 2.100(8) Ni-N (1C) Pt-N (1D) <

complexes. Metallophilic interactions are further suggested in the antiferromagnetic coupling between lanterns as discussed below.

Compounds 3–5 with L = pySMe were prepared in a similar manner as 1–2, with MCl₂·xH₂O instead of MSO₄·xH₂O as the metal source. The Co (3) and Ni (4) analogs, shown in Figs. S3 and S4, are isomorphous to the Fe-containing complex (2), and therefore also have two crystallographically independent dimers in the asymmetric unit. The B/C dimer in 3 has a Pt(1B)···Pt(1C) metallophilic interaction of 3.2737(7) Å and a longer Pt···S interaction of 3.968(3) Å (Table 1). The A/D dimer in the asymmetric unit of 3 has the second longest Pt(1A)···Pt(1D) interaction of 3.3977(7) Å (the longest is in 2) and Pt···S distance of 3.931(3) Å, and both dimers are in the staggered class as seen in the Fe analog. Similarly, isomorphous Ni-containing 4 has two staggered dimers, the C/D dimer with a Pt···Pt metallophilic interaction of 3.2198(6) Å and Pt···S of 3.7599(9) Å and the A/B dimer with a longer Pt···Pt interaction of 3.3212(6) Å and Pt···S of 3.8896(9) Å.

The Zn-containing compound (5) (Fig. S5) is most similar to the Mn analog (1) in that there is only one crystallographically independent molecule with non-bonding Pt---Pt interactions of 3.9165(3) Å and Pt···S intermolecular interactions of 3.1195(7) Å, falling into the square class. Along with 1, 6 (Fig. S6) is one of two new complexes containing Mn, in this case with the pyNH₂ terminal ligand. Single crystal X-ray diffraction studies of 6 show a non-bonding Pt...Pt interaction of 4.1413(3) Å and Pt...S interaction of 3.348(1) Å. Unlike 1, 6 has a M-Pt-Pt angle much closer to 145° and agrees with the previously observed trend shown in Fig. 2. Compound 7 was synthesized in the same manner as 6 using FeSO₄·7H₂O. Single crystal X-ray diffraction studies of 7, Fig. 1, revealed a typical monomeric lantern structure with a Pt-Fe bond distance of 2.6788(5) Å and a Pt---Pt non-bonded interaction of 4.1282(5) Å. Compound 7 falls into the square classification, like 1 and 6, which is characterized by shorter Pt...S contacts than Pt...Pt and a M-Pt-Pt angle around 140°.

Pt···Pt metallophilic interactions have been well studied in the literature, using either the Pt···Pt distance [40], luminescence [41,42], and/or the complexes' conductivity [43,44] to determine the presence of this interaction. For example, in potassium tetracyanoplatinates (KCPs), chains are formed through the stacking of square-planar [Pt (CN)₄]⁻² anions [45]. The electrical conductivities of these compounds have been determined and it has been shown that the longest Pt···Pt metallophilic interaction, or the longest distance in which there is

demonstrable d_z^2 orbital overlap, is approximately 3.3 Å for KCPs [46]. Work with dithiocarboxyate lantern complexes $[Pt_2(S_2CR)_4]$ $(R = CH_3,$ (CH₂)₄CH₃, or cyclohexyl) has shown that subtle changes in intermolecular Pt···Pt distances have a large effect on the resultant conductivities of compounds, with the most conductive being R = CH₃ with a distance of 3.138(1) Å and room temperature conductivity of $2 \times 10^{-3} \,\mathrm{S\,cm}^{-1}$. When the R group is bulkier (R = (CH₂)₄CH₃) the conductivity decreases to $0.9\times 10^{-3}\,\text{S}\,\text{cm}^{-1}$ while the Pt···Pt distance increases slightly to 3.141(1) Å. The correlation between conductivity and $Pt \cdot \cdot \cdot Pt$ distance is more distinctly shown when R = cyclohexyl; the Pt...Pt distance significantly increases to 3.339(2) Å with an almost negligible conductivity of $< 0.001 \times 10^{-3} \, \mathrm{S \, cm^{-1}}$ [45]. These results are in agreement with the maximum Pt···Pt interaction observed for KCPs of about 3.3 Å; any longer distances correspond to a drastic decrease in the resultant conductivity. In our previously reported complexes, we have argued the presence of Pt···Pt metallophilic interactions based on their distances, which range from 3.0583(4)-3.1261(3) Å, well within the ranges observed for KCPs and [Pt2(S2CR)4]. The structures in 2-4 all have one dimer within the demonstrated range for a metallophilic interaction and one outside of this range..

The only previous examples within our work of PtM lantern complexes having two crystallographically independent molecules within the asymmetric unit are the anionic complexes {Na(15C5)}[PtCo (SAc)₄(NCS)] and {Na(12C4)₂}[PtCo(SAc)₄(NCS)] which lack any Pt...Pt metallophilic interactions [15]. The lantern complexes in the 15crown-5 derivative exhibit a partially eclipsed geometry (see Scheme 2) with a difference of 0.008 Å between their Pt···Pt interactions whereas the molecules in the 12-crown-4 derivative are totally eclipsed and exhibit a difference of 0.008 Å. The difference in the intermolecular Pt distances between the dimers in 2, 3, and 4 are much more pronounced than seen in the Co-NCS complexes, with differences of 0.162, 0.124, and 0.101 Å respectively. The slightly different crystal packings seen in 2-4 resulting in multiple dimers are most likely due to a shallow potential energy surface existing among these four types of lantern conformations, leading to dimers with exceptionally long Pt···Pt metallophilic interactions. In fact, polymorphs of the dithiocarboxylates [Pt2(S2CR)4] have shown differences in these Pt interactions through choice of crystallization solvent [45]. A zig-zag chain can be synthesized in which the dimers have a square configuration with long Pt...Pt and short Pt...S interactions when crystallized from toluene, whereas linear chains with much closer Pt···Pt interactions are obtained through crystallization from CH₂Cl₂, leading to the hypothesis that solvent polarity plays a determining role in the dimer alignments [47].

All of our previously reported lantern complexes that exhibit Pt···Pt metallophilic contacts are within the staggered class. These include examples of complexes with both the acetate ligand used in this report [13] as well as the bulkier benzoate ligand [28]. The metallophilic interactions in the new series of pySMe based lantern complexes 2–4 range from 3.2198(6) to 3.2913(6) Å for the dimers with shorter interactions and 3.3212(6)–3.4533(6) Å for the dimers with longer interactions, as seen in Table 1. As one might expect, as the atomic number of the 3*d* metal decreases from Fe to Ni, the Pt···M distances decrease. Previously, greater antiferromagnetic coupling was seen in Ni cases than Co [13,28].

Because the steric bulk of these three lantern building blocks is virtually the same, the solid-state structural differences among these metallophilic dimers are likely to be influenced by several factors, whose relative influence is difficult to quantify [48]. These factors include the relative Lewis acid/base character of Pt and S in each lantern, dispersion effects, electronic character of the 3d metal, and intermolecular packing forces from the carboxylate substituent. An additional indicator of electronic communication between the dimers across the Pt---Pt contact is any magnetic interaction, which has been measured for 2–4, vide infra. Computational efforts are also underway with diamagnetic systems to assess the dispersion forces, relative Lewis acid-base character and packing influence of the carboxylate group.

4.2. Electronic spectroscopy

Previously made lantern complexes exhibit three types of electronic transitions: LMCT, *d-d* transitions, and intermetallic *d-d* charge transfer. All lantern complexes with the thioacetate backbone exhibit LMCT in the UV region around 260 nm, and the open-shell species have *d-d* transitions in the visible, and some intermetallic transitions in the near infrared region. In addition to the observed LMCT band, Mn-containing 1 and 6 display a very weak UV peak around 370 nm consistent with charge transfer, as seen in Fig. 4. The previously published anionic Pt-Mn containing lantern displayed a weak peak in the visible at 444 nm as

well as a weak NIR absorbance at 1159 nm [15], this NIR region was not measured in 1 or 6. The 370 nm absorbances in both 1 and 6 (Fig. S7) are blue shifted by about 80 nm compared to the visible peak observed in the previous Mn lantern.

Fe-containing **2** has a strong UV peak around 380 nm with a molar absorptivity of $3060\,\mathrm{M}^{-1}\mathrm{cm}^{-1}$ assigned to charge transfer, as seen in comparison with **2** in Fig. 4. In Fe-containing **7**, this peak is red shifted to 359 nm (Fig. S8). In our previously made [PtFe(tba)₄(OH₂)], a weak NIR absorbance at 996 nm was observed and attributed to intermetallic *d-d* charge transfer. A similar weak NIR peak around 970 nm observed in **2** as well, but this region was not measured in **7**.

Electronic spectra for 3–5 (Figs. S9–11) are consistent with our previously reported lantern complexes with M=Co, Ni, and Zn. All show a peak in the UV region around 260 nm assigned to LMCT from the thioacetate backbone to Pt center; for diamagnetic Zn-containing 5, this is the only peak [15]. Co-containing 3 displays two absorptions in the visible range around 500 nm and 524 nm that are assigned to d-d transitions on the Co center. Ni-containing 4 displays two weaker absorptions in the visible range around 673 nm and 830 nm. Both 3 and 4 show weak absorptions in the NIR as well, at 1383 nm and 1165 nm respectively, which suggest intermetallic d-d charge transfer.

4.3. Magnetic susceptibility

Solution state Evans method measurements [33,34] were performed for all complexes except Zn-containing 5. The spin-only predicted value for a high spin octahedral Mn(II) ion is 5.9, and Mn-containing 1 and 6 show susceptibility values of 5.8(1) and 5.9(1) respectively. Although commonly reported in units of Bohr magneton, μ_B , effective magnetic moments are unitless [37,38]. Both complexes are consistent with a high spin pseudo-octahedral oxygen ligated Mn(II) ion.

Fe-containing 2 and 7 show μ_{eff} values of 5.5(1) and 4.5(1) respectively. The predicted spin-only magnetic moment for a high spin octahedral Fe(II) complex is 4.90 and that for high spin Fe(III) is 5.92. Compound 2 has a value higher than predicted for Fe(II), but still within the common range. As seen with our previously published Co and Ni containing lantern complexes, our only other published Fe containing lantern, [PtFe(tba)₄(OH₂)] [28] also has a larger than

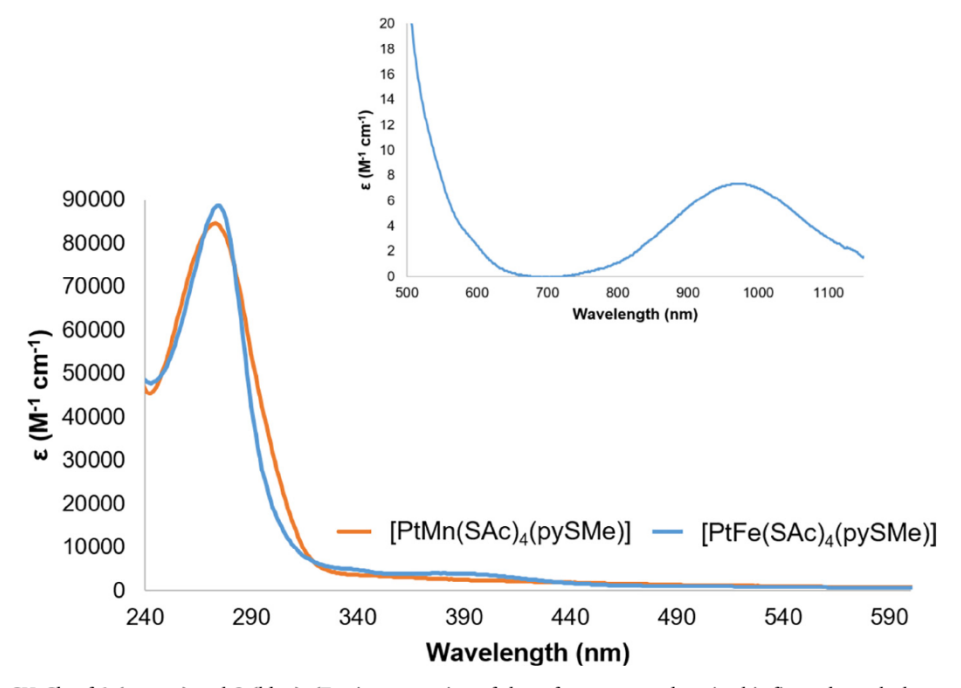


Fig. 4. UV-Vis spectra in CH₂Cl₂ of 1 (orange) and 2 (blue). (For interpretation of the references to colour in this figure legend, the reader is referred to the web version of this article.)

predicted spin-only magnetic moment of 5.11. Compound **7** is a bit unusual in that the experimental susceptibility is actually lower than the predicted spin only value, but this value is still within the range of observed species for a high spin Fe(II) complex.

These solution susceptibility values of 5.2(1) (3) and 3.8(1) (4) for the Co and Ni-containing complexes are both consistent with high spin first-row transition metal centers with oxygen carboxylate donors and a pseudo-octahedral geometry. The predicted spin-only magnetic moment for a high spin Co(II) complex is 3.88, however higher than expected magnetic moments are often observed in Co complexes due to their spin orbit coupling. Our previous Co-containing complexes have had higher than predicted susceptibility values, ranging from 4.61 for L = py [29] and 5.06 for $L = pyNO_2$ [13] so this larger value for 3 is not surprising. Similarly, for Ni-containing 4, the larger than predicted value of 2.83 is not unreasonable, as seen previously with L = py having a susceptibility value of 3.15. The solid-state susceptibility data, however, suggest that there may be dimers in solution, vide infra.

Variable-temperature magnetic properties of solid-state samples of the heterobimetallic {PtM} lantern complexes **2** (M = Fe), **3** (M = Co), and **4** (M = Ni), those with staggered dimeric configurations, were collected between 2 K and 300 K. Treating compounds **2–4** as monomeric species (Figs. S22–S24), all three compounds give room-temperature $\chi_M T$ values that correspond roughly with four, three, and two unpaired electrons, respectively. As the temperature is decreased, all three compounds show decreasing $\chi_M T$ values that trend toward 0 cm³ Kmol⁻¹. For the putative half-integer spin system expected for the Co-containing compound, this result only makes sense if antiferromagnetic coupling is operative. Treating the compounds as "dimeric" {MPt}···{PtM} entities gives temperature-dependent magnetic susceptibility behavior consistent with previous measurements and interpretations of {MPt} lantern complexes (Fig. 5).

Interestingly, a comparison of room-temperature solid-state and solution magnetic data (Table 2) suggests that the Fe- and Co-containing compounds behave as monomers in solution, while the Ni analogue is more like a dimer. Measured susceptibility values support designations of high spin Fe(II) (S=2), high spin Co(II) (S=3/2) and high spin Ni(II) (S=1) species.

In order to gain more insight into possible magnetic interactions between lantern species, temperature-dependent magnetic property curves were fit using PHI [36], and best fit parameters are collected in Table 3. Compounds 2–4 were modeled as dimers and are denoted as

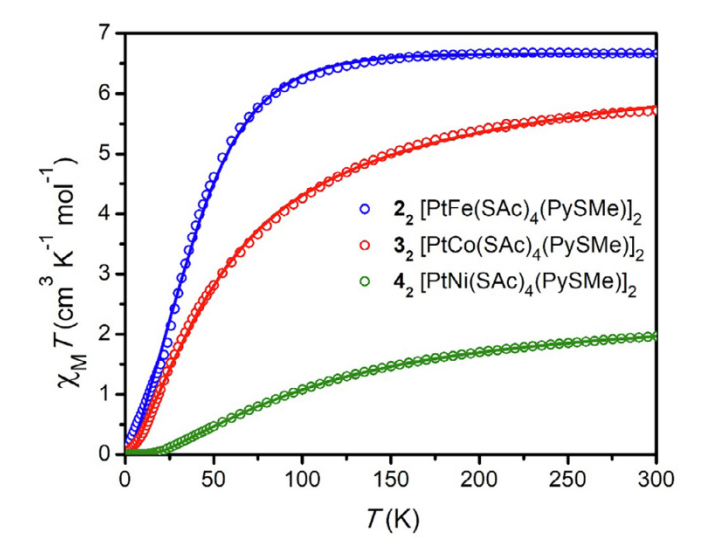


Fig. 5. Temperature dependence of magnetic susceptibility-temperature products for solid state samples of 2-4, collected at $10\,\mathrm{kOe}$. Each compound was treated as a dimeric $\{\mathrm{PtM}\}_2$ species. Solid lines designate best fits with parameters provided in Table 2.

Table 2Solution and room-temperature solid-state (300 K, 10 kOe) effective magnetic moment values.

Formula	Compound	Solution	Solid-state (SQUID), μ_{eff}	
	(Evans), μ_{eff}		Monomer	Dimer
[PtFe(SAc) ₄ (pySMe]	2	5.45	5.01	7.30
[PtCo(SAc) ₄ (pySMe]	3	5.24	4.91	6.76
[PtNi(SAc) ₄ (pySMe]	4	3.82	2.91	3.97

Table 3
Results of fits of magnetic susceptibility for 2–4 utilizing PHI.

	2_{2}	3_{2}	42
giso	2.05*	2.61	2.18
$J \text{ (cm}^{-1})$	-6.7	-8.8	-30.7
TIP ($\times 10^{-6}$ emu K mol ⁻¹)	670	1000^*	280
zJ (cm ⁻¹)	2.41	-0.08	0.016
Paramagnetic Impurity (%)	6.2	4.5*	0.5*
	(S = 2)	(S = 3/2)	(S = 1)
fa	0.50216	0.15405	0.00038

- ^a Sum of the residuals squared.
- * Value was held constant.

2₂, **3**₂, and **4**₂. As some of us have previously shown, for face-to-face {MPt} units with the staggered conformation, antiferromagnetic coupling between the two {PtM} centers leads to S = 0 ground states [28,29]. Qualitatively, we note that the downturn in $\chi_M T$ values tracks with M(3d)···M(3d) distances determined from crystallographic data, in which longer distances lead to a lower temperature for decrease in $\chi_M T$, consistent with weaker inter-lantern magnetic interactions.

For 4, the magnetic susceptibility data model best as two [PtNi (SAc)₄(pySMe)] molecules antiferromagnetically coupling as a dimer, as models of 4 as a monomer utilizing anisotropy parameters D and E generate a much higher sum of residuals squared values (Table S10). Truncations of the data at various temperatures based on features observed in the $\chi_{\rm M}$ vs T plot (Fig. S20) produce very little change in both the coupling constant and fit quality (Table S10). These interactions are on the same order of magnitude as previously reported {PtNi} dimers [28,29]. The small Curie tail observed at $T < 10~{\rm K}$ is modeled with a 0.5% paramagnetic impurity, producing negligible changes to the fits. There is negligible coupling between dimers.

For 3, the temperature dependence of the solid-state magnetic susceptibility data also models best as a dimer. Unlike Ni-containing 4, the fit parameters were somewhat more sensitive to the choice of truncation temperature (Table S11), likely due to inherent complexity of the electronic structure for high spin Co(II) ions. Fits were satisfactory at modeling the low temperature data upon constraining temperature-independent paramagnetism (TIP) to $1000 \times 10^{-6} \, \mathrm{emu} \, \mathrm{K} \, \mathrm{mol}^{-1}$. This value was chosen as previous {PtM} dimers exhibit large TIP [28,29]. The coupling between two {CoPt} lanterns in 3 is approximately $-9 \, \mathrm{cm}^{-1}$, only about one third of the strength of the coupling found in 4. Like the Ni-containing analogue, there is little coupling between dimers. Previously studied {PtM} lantern complexes also show larger coupling constants between Ni versus Co [39].

For consistency with the treatment of the other compounds, we fit magnetic susceptibility data for the Fe-containing compound ${\bf 2}$ as a dimer. Observing non-linear behavior in the ${\bf M}$ vs ${\bf H}$ plot (Fig. S12), we suspect that a small amount of ferromagnetic impurity is present in the sample which complicates the data analysis. Additionally, the $\chi_{\rm M}$ vs ${\bf T}$ plot (Fig. S16) shows several discontinuities at low temperature, possibly relating to paramagnetic impurities or long-range ordering; either scenario further complicates fits based solely on magnetic exchange within the dimer. Fits without constraints yield nonsensical values (e.g., ${\bf g}_{\rm iso} < 2$, negative TIP values, ${\bf S} = 2$ impurity greater than 10%), and

thus require several values to be constrained (Table S12). Thus, fit values for this compound should be considered as qualitative rather than quantitative. Comparing 2 to 3, the best fit intra-dimer coupling values are similar in magnitude, and much smaller than that found for Ni-containing 4. Interestingly, the inter-dimer mean field coupling (*zJ*) is an order of magnitude larger for 2 than 3, suggesting a competition between {FePt}····{PtFe} dimer exchange and antiferromagnetic coupling or even ordering in the bulk sample.

5. Conclusions:

A new series of heterobimetallic lantern complexes axially bound with para-pySMe has been synthesized and characterized with M=Mn (1), Fe (2), Co (3), Ni (4), and Zn (5). The previously published lantern series, $[PtM(SAc)_4(pyNH_2)]$, has also been expanded to include both Mn (6) and Fe (7) analogs. The new Mn-containing lanterns, 1 (L = pySMe) and 6 (L = pyNH₂), are the first examples of an electrostatically neutral lantern compound containing both Pt and Mn as well as being fully crystallographically characterized.

The Fe-containing complexes 2 and 7, as well as our previously published [PtFe(tba)₄(OH₂)] [28], are the only examples of a lantern structure containing both Pt and Fe. Compounds 2 and 7 are therefore the first examples with the thioacetate backbone. Our published Fe lantern complexes are the only examples of paramagnetic Fe-containing heterobimetallic lantern species. The paramagnetism as well as control over the axially bound ligand can be exploited to form 1D arrays with both interesting electronic and magnetic properties, both of which are currently being explored by our group.

New pySMe ligated lantern complexes were also synthesized with M = Co (3), Ni (4), and Zn (5). When comparing the complexes in this new family to our previously published structures, it was found that, for the same 3d elements, 1-4 all have generally comparable electronic, structural, and magnetic properties with the lantern building blocks. The pseudo-octahedral geometry and thiocarboxylate oxygen-ligated 3d metal centers are expected to yield higher than spin-only μ_{eff} values for all of our late-metal complexes, however, a slight lowering of the susceptibility is observed for pyNH2 ligated 7 (Fe), but is still within range for a high spin pseudo-octahedral oxygen ligated Fe(II). Intermolecularly, a very interesting pair of dimers were observed in 2, 3, and 4. In each case, one dimer displays Pt...Pt metallophilic interactions within the normal distance range while the other exhibits much longer metallophilic distances. Thus far these exceptionally long metallophilic contacts have only been observed when L = pySMe. Nevertheless, the variable temperature magnetic susceptibility data of 2-4 suggest antiferromagnetic coupling across these Pt···Pt contacts. The coupling magnitudes in 3 and 4 are decreased compared to Co- and Ni-containing lantern complexes previously measured with shorter Pt...Pt contacts, also consistent with AF coupling across the metallophilic interaction. This measurement of 2 is the first time this phenomenon has been observed in a {PtFe} member of this family.

To determine the steric contributions of this type of crystal packing, the thiobenzoate derivatives will also be synthesized and evaluated. The future linkage of these discrete units into 1D arrays with control over the magnetic and electronic properties as well as the conductivity of the individual lantern units are currently being studied within the group.

Acknowledgements

We thank NSF-CHE 0619339 (NMR spectrometer at Boston University), NSF-CCT EMT 08-517 (L.H.D.), NSF-CHE 1800554 (M.P.S. and R.I.P.) and Boston University UROP (L.A.Z.) for financial support.

Appendix A. Supplementary data

Supplementary data to this article can be found online at https://

doi.org/10.1016/j.ica.2019.04.054.

References

- [1] C. Slabbert, M. Rademeyer, One-dimensional halide-bridged polymers of metal cations with mono-heterocyclic donor ligands or cations: a review correlating chemical composition, connectivity and chain conformation, Coord. Chem. Rev. 288 (2015) 18–49.
- [2] F.A. Cotton, C.A. Murillo, R.A. Walton, Multiple Bonds Between Metal Atoms, Springer Science & Business Media, 2005.
- [3] J.F. Berry, F.A. Cotton, P. Lei, T. Lu, C.A. Murillo, Additional steps toward molecular scale wires: further study of Ni510/11+ chains embraced by polypyridylamide ligands, Inorg. Chem. 42 (11) (2003) 3534–3539.
- [4] J.W. Bray, L.V. Interrante, I. Jacobs, J.C. Bonner, Extended linear chain compounds, Plenum, New York 3 (1983) 353.
- [5] E. Coronado, J.R. Galán-Mascarós, C.J. Gómez-García, C. Martí-Gastaldo, Synthesis, structure, and magnetic properties of the oxalate-based bimetallic ferromagnetic chain {[K (18-crown-6)][Mn (H2O) 2Cr (ox) 3]} ~ (18-crown-6 = C12H24O6, ox = C2O42-), Inorg. Chem. 44 (18) (2005) 6197–6202.
- [6] G. Givaja, P. Amo-Ochoa, C.J. Gómez-García, F. Zamora, Electrical conductive coordination polymers, Chem. Soc. Rev. 41 (1) (2012) 115–147.
- [7] Y.-Z. Zheng, Z. Zheng, X.-M. Chen, A symbol approach for classification of molecule-based magnetic materials exemplified by coordination polymers of metal carboxylates, Coord. Chem. Rev. 258–259 (2014) 1–15.
- [8] W. Krause, S. Achilefu, Contrast Agents II: Optical, Ultrasound, X-Ray Imaging and Radiopharmaceutical Imaging vol. 222, (2002).
- [9] S.M. Drew, D.E. Janzen, C.E. Buss, D.I. MacEwan, K.M. Dublin, K.R. Mann, An electronic nose transducer array of vapoluminescent platinum (II) double salts, J. Am. Chem. Soc. 123 (34) (2001) 8414–8415.
- [10] R.L. White-Morris, M.M. Olmstead, A.L. Balch, Aurophilic interactions in cationic gold complexes with two isocyanide ligands. Polymorphic yellow and colorless forms of [(cyclohexyl isocyanide) 2AuI](PF6) with distinct luminescence, J. Am. Chem. Soc. 125 (4) (2003) 1033–1040.
- [11] A.L. Balch, Polymorphism and luminescent behavior of linear, two-coordinate gold (I) complexes, Gold Bull. 37 (1–2) (2004) 45–50.
- [12] J.K. Bera, K.R. Dunbar, Chain compounds based on transition metal backbones: new life for an old topic, Angew. Chem. Int. Ed. 41 (23) (2002) 4453–4457.
- [13] F.G. Baddour, S.R. Fiedler, M.P. Shores, J.A. Golen, A.L. Rheingold, L.H. Doerrer, Heterobimetallic lantern complexes that couple antiferromagnetically through noncovalent Pt-Pt interactions, Inorg. Chem. 52 (9) (2013) 4926–4933.
- [14] W. Chen, F. Liu, T. Nishioka, K. Matsumoto, Heterotrimetallic complexes [{Pt (RNH2)2(μ-NHCOtBu)2}2M](ClO4)n (M = Mn Co, Cu, Ni, Cd, and Zn, n = 2; M = In, n = 3),[{Pt (NH3)(μ-DACHCOtBu)(μ-NHCOtBu)}2Ni](ClO4)2, and [{Pt (RNH2)2(NHCOtBu)2}3Ag3](ClO4)3 bridged by amidate ligands: a novel amidate amine interligand reaction during the Pt–Ni bond formation, Eur. J. Inorg. Chem. 2003 (23) (2003) 4234–4243.
- [15] J.L. Guillet, I. Bhowmick, M.P. Shores, C.J.A. Daley, M. Gembicky, J.A. Golen, A.L. Rheingold, L.H. Doerrer, Thiocyanate-ligated heterobimetallic ptm lantern complexes including a ferromagnetically coupled 1D coordination polymer, Inorg. Chem. 55 (16) (2016) 8099–8109.
- [16] N.S. Akhmadullina, N.V. Cherkashina, N.Y. Kozitsyna, I.P. Stolarov, E.V. Perova, A.E. Gekhman, S.E. Nefedov, M.N. Vargaftik, I.I. Moiseev, Synthesis of palladium (II) 3d-metal(II) paddlewheel acetate-bridged heterodimetallic complexes: unexpected catalysis by water molecules, Inorg. Chim. Acta 362 (6) (2009) 1943–1951.
- [17] P.L. Dunn, R.K. Carlson, I.A. Tonks, Synthesis and characterization of triply-bonded titanium-iron complexes supported by 2-(diphenylphosphino)pyrrolide ligands, Inorg. Chim. Acta 460 (2017) 43–48.
- [18] C.R. Groom, I.J. Bruno, M.P. Lightfoot, S.C. Ward, The cambridge structural database, Acta Cryst. Sect. B 72 (2) (2016) 171–179.
- [19] E. Reisner, J. Telser, S.J. Lippard, A planar carboxylate-rich tetrairon(II) complex and its conversion to linear triiron(II) and paddlewheel diiron(II) complexes, Inorg. Chem. 46 (25) (2007) 10754–10770.
- [20] S. Yoon, S.J. Lippard, Water affects the stereochemistry and dioxygen reactivity of carboxylate-rich diiron(II) models for the diiron centers in dioxygen-dependent non-heme enzymes, J. Am. Chem. Soc. 127 (23) (2005) 8386–8397.
- [21] M. Nippe, E. Bill, J.F. Berry, Group 6 complexes with iron and zinc heterometals: understanding the structural, spectroscopic, and electrochemical properties of a complete series of MM···M′ compounds, Inorg. Chem. 50 (16) (2011) 7650–7661.
- [22] M. Nippe, J. Wang, E. Bill, H. Hope, N.S. Dalal, J.F. Berry, crystals in which some metal atoms are more equal than others: inequalities from crystal packing and their spectroscopic/magnetic consequences, J. Am. Chem. Soc. 132 (40) (2010) 14261–14272.
- [23] Y.-S. Ma, X.-Y. Tang, F.-F. Xue, B. Chen, Y.-L. Dai, R.-X. Yuan, S. Roy, Structural diversity and magnetic properties of the manganese(II)/carbazol-9-ylacetate/N,N'-donor reaction system, Eur. J. Inorg. Chem. 2012 (8) (2012) 1243–1249.
- [24] M. Fontanet, M. Rodríguez, X. Fontrodona, I. Romero, F. Teixidor, C. Viñas, N. Aliaga-Alcalde, P. Matějíček, Water-soluble manganese inorganic polymers: the role of carborane clusters and producing large structural adjustments from minor molecular changes, Chem. Eur. J. 20 (43) (2014) 13993–14003.
- [25] Z. Chen, Y. Ma, F. Liang, Z. Zhou, Synthesis, crystal structure, and magnetic properties of two manganese(II) polymers bearing ferrocenecarboxylato ligands, Eur. J. Inorg. Chem. 2007 (14) (2007) 2040–2045.
- [26] H. Chen, D. Xiao, J. He, Z. Li, G. Zhang, D. Sun, R. Yuan, E. Wang, Q.-L. Luo, A series of novel entangled coordination frameworks with inherent features of self-

- threading, polyrotaxane and polycatenane, CrystEngComm 13 (15) (2011)
- [27] Y. Lou, J. Wang, Y. Tao, J. Chen, A. Mishima, M. Ohba, Structure modulation of manganese coordination polymers consisting of 1,4-naphthalene dicarboxylate and 1,10-phenanthroline, Dalton Trans. 43 (22) (2014) 8508–8514.
- [28] E.W. Dahl, F.G. Baddour, S.R. Fiedler, W.A. Hoffert, M.P. Shores, G.T. Yee, J.-P. Djukic, J.W. Bacon, A.L. Rheingold, L.H. Doerrer, Antiferromagnetic coupling across a tetrametallic unit through noncovalent interactions, Chem. Sci. 3 (2) (2012) 602–609.
- [29] F.G. Baddour, S.R. Fiedler, M.P. Shores, J.W. Bacon, J.A. Golen, A.L. Rheingold, L.H. Doerrer, Pt-Pt vs. Pt-S contacts between pt-containing heterobimetallic lantern complexes, Inorg. Chem. 52 (23) (2013) 13562–13575.
- [30] G.B. Kauffman, J.J. Thurner, D.A. Zatko, Ammonium hexachloroplatinate (IV), Inorg. Synth. 9 (1967) 182–185.
- [31] R.N. Keller, Potassium tetrachloroplatinate(II) (potassium chloroplatinite), Inorg. Synth. 1946, II, 247–250.
- [32] G.B. Kauffman, D.O. Cowan, cis-and trans-Dichlorodiammineplatinum(II), Inorg. Syn. (Jacob Kleinberg, editor. McGraw) 7 (1963) 239–245.
- [33] D. Evans, The determination of the paramagnetic susceptibility of substances in solution by nuclear magnetic resonance, J. Chem. Soc. (Resumed) (1959, 2003–2005.).
- [34] S.K. Sur, Measurement of magnetic susceptibility and magnetic moment of paramagnetic molecules in solution by high-field Fourier transform NMR spectroscopy, J. Magnet. Resonance (1969) 82 (1) (1989) 169–173.
- [35] G.A. Bain, J.F. Berry, Diamagnetic corrections and Pascal's constants, J. Chem. Educ. 85 (4) (2008) 532.
- [36] N.F. Chilton, R.P. Anderson, L.D. Turner, A. Soncini, K.S. Murray, PHI: A powerful new program for the analysis of anisotropic monomeric and exchange-coupled polynuclear d- and f-block complexes, J. Comput. Chem. 34 (13) (2013)

- 1164-1175.
- [37] J.I. Hoppe, Effective magnetic moment, J. Chem. Educ. 49 (7) (1972) 505.
- [38] S. Kettle, Magnetic properties of transition metal complexes, Physical Inorganic Chemistry, Springer, 1996, pp. 185–210.
- [39] S.A. Beach, L.H. Doerrer, Heterobimetallic lantern complexes and their novel structural and magnetic properties, Acc. Chem. Res. 51 (5) (2018) 1063–1072.
- [40] P. Pyykkö, Strong closed-shell interactions in inorganic chemistry, Chem. Rev. 97 (3) (1997) 597–636.
- [41] E.M. Gussenhoven, M.M. Olmstead, J.C. Fettinger, A.L. Balch, Interplay of supramolecular organization, metallophilic interactions, phase changes, and luminescence in four polymorphs of IrI(CO)2(OC(CH3)CHC(CH3)N(p-tol)), Inorg. Chem. 47 (11) (2008) 4570–4578.
- [42] M. Gil-Moles, M.C. Gimeno, J.M. López-de-Luzuriaga, M. Monge, M.E. Olmos, D. Pascual, Tailor-made luminescent polymers through unusual metallophilic interaction arrays Au···Ag···Ag, Inorg. Chem. 56 (15) (2017) 9281–9290.
- [43] J.S. Miller, Extended Linear Chain Compounds vol. 3, (2012).
- [44] J.S. Miller, A.J. Epstein, One-dimensional inorganic complexes, Prog. Inorg. Chem. (1976) 1–151.
- [45] A. Guijarro, O. Castillo, A. Calzolari, P.J.S. Miguel, C.J. Gómez-García, R. di Felice, F. Zamora, Electrical conductivity in platinum-dimer columns, Inorg. Chem. 47 (21) (2008) 9736–9738.
- [46] A. Kobayashi, T. Kojima, R. Ikeda, H. Kitagawa, Synthesis of a one-dimensional metal-dimer assembled system with interdimer interaction, M2 (dtp) 4 (M = Ni, Pd; dtp = dithiopropionato), Inorg. Chem. 45 (1) (2006) 322–327.
- [47] C. Bellitto, A. Flamini, O. Piovesana, P. Zanazzi, Metal-metal interactions in one dimension. 3. Segregated canted stacks of tetrakis (dithioacetato) diplatinum (II), Inorg. Chem. 19 (12) (1980) 3632–3636.
- [48] S. Alvarez, A cartography of the van der Waals territories, Dalton Trans. 42 (24) (2013) 8617–8636.